

Strong lensing, cosmology and lensing halos

Edvard Mörtsell and Christoffer Sunesson

Department of Astronomy, Stockholm University, SE-106 91 Stockholm, Sweden

E-mail: edvard@astro.su.se, sunesson@astro.su.se

Abstract. With future wide and deep cosmological sky surveys, a large number of gravitationally lensed, multiply imaged systems will be found. In addition to multiply imaged galaxies and quasars, sources will include transient events like supernovae and gamma ray bursts in which case very accurate time delay measurements are possible. Also, large numbers of systems with several lensed sources behind a single lens will be observed. In this paper, we review and compare different possibilities of using future strong lensing data to probe lens matter distributions and to determine the Hubble parameter and the matter density of the universe. Specifically, we investigate the possibility to break the well-known degeneracy between dark matter halo profiles and the Hubble parameter using observed flux ratios. We also investigate how strong lensing can provide useful constraints on the matter density of the universe independently of the flux ratios and other cosmological probes.

1. Introduction

In the last decade, a picture of our universe being dominated by dark energy and dark matter has emerged. Elements of this picture include observations of Type Ia supernova (SNIa) distances [1–4], anisotropies in the cosmic microwave background (CMB) [5–10] and the large scale structure (LSS) of galaxies [11, 12]. For a recent concise review of cosmological bounds on dark matter and dark energy, see Ref. [13]. A flat universe with $\Omega_\Lambda \sim 0.7$ and $\Omega_M \sim 0.3$ provides a good fit to all current observations, indicating a recent ($z \sim 0.5$) transition from a decelerating universal expansion to an accelerating universal expansion. The current expansion rate (and hence overall scale) of the universe as measured by the Hubble Space Telescope (HST) Key Project [14] is $h = 0.72 \pm 0.08$ where h is the dimensionless Hubble constant, $h = H_0/(100 \text{ km s}^{-1} \text{ Mpc}^{-1})$.

Though the picture described above is very effective in explaining all observational data with just a few free parameters, the nature of the dark energy and dark matter is still unknown. The simplest dark energy model is the cosmological constant. Difficulties in theoretically explaining the magnitude of the energy density has brought about a large number of alternative explanations, including quintessence [15–17], k-essence [18, 19] and phantom energy [20, 21]. However, current observations are still best explained by the cosmological constant [22, 23].

On large scales, dark matter is well-described as being non-relativistic and collisionless, i.e. cold dark matter (CDM). On galaxy scales however, there has been a dispute whether there is a discrepancy between numerical simulations of galaxy formation in CDM models [24–28] and observations of rotation curves of dark matter dominated galaxies [29–31]. Precise observational determinations of halo density profiles will help in understanding whether there is any contradiction with the simulations and provide further insight into the properties of dark matter.

When investigating the matter distribution of the universe, gravitational lensing has the advantage of being equally sensitive to all kinds of matter, regardless of its microscopic properties (e.g. being baryonic or non-baryonic) and dynamical state. Both strong lensing (multiply imaged sources) and weak lensing (weakly distorted source images) has been used to constrain the matter distribution in galaxy scale [32–34] and cluster scale [35–38] halos.

Besides being able to provide information on the matter distribution of dark matter halos, gravitational lensing has also the potential to constrain cosmological parameters such as Ω_M , Ω_Λ and h . More than 40 years ago, Refsdal showed how the time delay between multiple images of supernovae (SNe) could be used to measure h and the mass of the lensing galaxy [39]. To date – for galaxy mass lenses – approximately 100 multiply imaged sources (including galaxies and quasars) have been observed out of which there are eleven well-determined time delay measurements (all quasars) [32, 40, 41]. For several reasons, it has been difficult to implement Refsdal’s method. First, time delays between quasar images are notoriously difficult to measure compared to what would be the case for transient sources like supernovae. Second, there is a degeneracy between the derived value of h and the matter distribution of the lensing galaxy. Modeling the lenses as more concentrated gives larger values of h and vice versa [42, 43].

Weak lensing can be used to probe the matter distribution of the universe also on very large scales. For reviews on the current state of cosmological constraints from LSS weak lensing, see Refs. [44–46]. There has also been attempts to constrain Ω_Λ through the statistics of gravitationally lensed quasars with disparate results [47–50].

Future strong lensing data will include observations from e.g. Pan-STARRS‡, the Large Synoptic Survey Telescope (LSST)§, the Joint Dark Energy Mission (JDEM) contender the Supernova Acceleration Probe (SNAP)|| and the James Webb Space Telescope (JWST)¶. In this note, we use simulated strong lensing data for a SNAP like mission combined with follow up observations from, e.g. JWST to investigate and compare different possibilities of constraining the slope of lens density profiles, the Hubble parameter and the matter density of the universe.

In Sec. 2 we present our lens model. In Sec. 3, we investigate different uses of a data set consisting of a large number of lens systems, each with a multiply imaged source

‡ <http://www.pan-starrs.org>

§ <http://www.lsst.org>

|| <http://snap.lbl.gov>

¶ <http://www.jwst.nasa.gov>

with well-determined time delay. This section extends and generalizes earlier work in Refs. [51] and [52] (see also Refs. [53–56]). In Sec. 4, we compare our results with what can be obtained by studying lens systems with several multiply lensed sources in a single lens (cf. the case of Abell 1689 [36]), with or without measured time delays. Finally, Sec. 5 contains a summary and a discussion of our results.

The cosmology used in the simulations throughout this paper is $h = 0.65$, $\Omega_M = 0.3$ and $\Omega_\Lambda = 0.7$. Our default dark matter halo is the singular isothermal sphere described in Sec. 2.

2. Lens model

The lens equation relating the angular source position $\vec{\theta}$ and the angular image position $\vec{\beta}$ is given by [57]

$$\vec{\beta}D_s = \vec{\theta}D_s - \hat{\alpha}D_{ls}, \quad (1)$$

where $\hat{\alpha}$ is the light deflection angle and D_{ls} , D_l and D_s are angular diameter distances between source and lens, lens and observer, and source and observer, respectively. The lens equation can be rewritten in dimensionless form by introducing an arbitrary length scale ξ_0 in the lens plane and a corresponding length scale $\eta_0 = \xi_0 D_s / D_d$ in the source plane. In terms of the dimensionless vectors $\vec{x} = \vec{\theta}D_l / \xi_0$ and $\vec{y} = \vec{\beta}D_s / \eta_0$ the lens equation takes the form

$$\vec{y} = \vec{x} - \vec{\alpha}(\vec{x}), \quad (2)$$

where

$$\vec{\alpha}(\vec{x}) = \frac{D_d D_{ls}}{D_s \xi_0} \hat{\alpha}(\xi_0 \vec{x}) \quad (3)$$

is the scaled deflection angle.

In this paper, we assume that the matter distribution in lenses can be described by a simple power-law density profile

$$\rho(r) \propto r^{-\eta}. \quad (4)$$

Since almost all images of multiply lensed sources are at a limited range of small r , this is a good approximation despite the fact that the slope is expected to change with radius at large r [24–27]. Note that the baryonic contribution to the density profile of lensing galaxies is non-negligible at small radii and that results from strong lensing not necessarily reflect the nature of pure dark matter halos.

For $\eta = 2$, we obtain the familiar singular isothermal sphere (SIS) model built upon the assumption that the mass components behave like particles in an ideal gas, confined by their spherically symmetric gravitational potential;

$$\rho_{SIS}(r) = \frac{v^2}{2\pi G} \frac{1}{r^2}. \quad (5)$$

Here, v is the line-of-sight velocity dispersion of the mass particles.

For all lensing purposes in this paper, matter distributions can be described by the projected Newtonian gravitational potential

$$\Psi = \frac{2D_l D_{ls}}{c^2 D_s \xi_0^2} \int \Phi dl. \quad (6)$$

For the power-law density profile, the projected potential is given by [40]

$$\Psi \propto x^{3-\eta} \quad (7)$$

where x is the impact parameter (in arbitrary units, ξ_0), i.e. the minimum distance between the light ray and the lens centre.

2.1. The Einstein radius

Since the scaled deflection angle $\vec{\alpha} = \nabla \Psi$, for a spherically symmetric lens we have

$$\Psi = \frac{x_E^{\eta-1}}{3-\eta} x^{3-\eta}, \quad (8)$$

where x_E is the Einstein radius; the solution to the lens equation for $y = 0$. The lens equation for the power-law lens can then be written (where $x > 0$ and α is directed towards the center of the lens)

$$y = x - \alpha = x - x_E^{\eta-1} x^{2-\eta}. \quad (9)$$

For multiple images, we have

$$y = x_1 - \alpha_1 = \alpha_2 - x_2 \quad (10)$$

and

$$x_E = \left[\frac{x_1 + x_2}{x_1^{2-\eta} + x_2^{2-\eta}} \right]^{\frac{1}{\eta-1}}. \quad (11)$$

Putting $\xi_0 = D_l$, i.e. denoting positions in terms of angles, we get

$$\theta_E = 2 \left[\frac{(\theta_1 + \theta_2)^{2-\eta}}{\theta_1^{2-\eta} + \theta_2^{2-\eta}} \right]^{\frac{1}{\eta-1}} \theta_{\text{SIS}}, \quad (12)$$

where θ_{SIS} is the Einstein radius for a SIS halo,

$$\theta_{\text{SIS}} = 4\pi \left(\frac{v}{c} \right)^2 \frac{D_{ls}}{D_s}. \quad (13)$$

2.2. Time delay

The time delay for a gravitationally lensed image as compared to an undeflected image is in the general case given by [57]

$$T = \frac{\xi_0^2 D_s}{D_l D_{ls}} (1 + z_l) \left[\frac{(\mathbf{x} - \mathbf{y})^2}{2} - \Psi \right]. \quad (14)$$

The time delay between two lensed images is given by $\Delta t = T_2 - T_1$. For an isothermal lens, we have

$$\Delta t_{\text{SIS}} = \frac{1}{2} \frac{D_l D_s}{D_{ls}} (1 + z_l) (\theta_1^2 - \theta_2^2) = 2\hat{\alpha} D_l (1 + z_l) \beta. \quad (15)$$

Note that the time delay is independent of the source redshift. In the general case of $\eta \neq 2$, we can rewrite Eq. (14) in terms of $q \equiv \Delta\theta / \langle \theta \rangle$ where $\Delta\theta = \theta_1 - \theta_2$ and $\langle \theta \rangle = (\theta_1 + \theta_2)/2$ and Taylor expand to obtain (see also Refs. [40] and [58])

$$\begin{aligned} \Delta t &= \frac{(\eta - 1) D_l D_s}{2 D_{ls}} (1 + z_l) (\theta_1^2 - \theta_2^2) \left[1 - \frac{(2 - \eta)^2}{12} q^2 + \mathcal{O}(q^3) \right] \\ &\simeq (\eta - 1) \Delta t_{\text{SIS}} \left[1 - \frac{(2 - \eta)^2}{12} q^2 \right]. \end{aligned} \quad (16)$$

There is a strong degeneracy between $\eta - 1$ and h (which comes in through the distances). This degeneracy can be broken by including data from the observed image luminosities; the flux ratio.

2.3. Flux ratio

We denote the flux ratio $r \equiv |\mu_1/\mu_2|$. The magnification μ for a source at position y observed at position x is given by

$$|\mu| = \left| \frac{x dx}{y dy} \right|. \quad (17)$$

For a power-law lens, we can express the flux ratio as

$$\begin{aligned} r &= \left| \frac{\theta_1}{\theta_2} \right| \left| \frac{1 - (2 - \eta)\theta_2^{1-\eta}(\theta_1 + \theta_2)/(\theta_1^{2-\eta} + \theta_2^{2-\eta})}{1 - (2 - \eta)\theta_1^{1-\eta}(\theta_1 + \theta_2)/(\theta_1^{2-\eta} + \theta_2^{2-\eta})} \right| \\ &= r_{\text{SIS}} \left| \frac{1 - (2 - \eta)\theta_2^{1-\eta}(\theta_1 + \theta_2)/(\theta_1^{2-\eta} + \theta_2^{2-\eta})}{1 - (2 - \eta)\theta_1^{1-\eta}(\theta_1 + \theta_2)/(\theta_1^{2-\eta} + \theta_2^{2-\eta})} \right|. \end{aligned} \quad (18)$$

Expanding this to second order in q , we obtain

$$r \simeq 1 + (\eta - 1)q + \frac{1}{2}(\eta - 1)^2 q^2 + \mathcal{O}(q^3). \quad (19)$$

Note that the flux ratio is independent of the value of h .

3. Individual multiple image systems

With a SNAP like JDEM contender, a large number of core collapse supernovae (CC SNe) will be discovered [59]. Monte Carlo simulations performed using the SNOC package [60] predicts that out of a total of $\sim 10^6$ CC SNe at $z < 5$ in a 20 square degree field during three years [61], ~ 850 will be multiply imaged with an I-band or J-band peak brightness < 28.5 mag for the dimmest image⁺. We demand that the surface brightness of the lens galaxy is fainter than 24 I magnitudes per square arcsecond at the position of the faintest image, in order to avoid contamination from the lens galaxy. In accordance with Ref. [52], we also introduce a quality factor, f , giving the fraction of the lens systems that are “simple”, i.e. a single dominant deflector with moderate

⁺ Since these simulations were performed, the SNAP specifications has been slightly degraded and the corresponding point-source magnitude limit is now 27.7. This number would yield ~ 400 multiply imaged CC SNe.

ellipticity and external shear. In the following, we assume a quality factor, $f = 0.5$, in accordance with currently observed systems [40]. This cut leaves a total of ~ 400 systems.

Here, we investigate how measurements of the image positions, time delays, flux ratios and lens galaxy properties for such systems could be used to constrain the slope of lens density profiles, η , the Hubble parameter, h , and the matter density of the universe, Ω_M .

3.1. Error budget

Our error assumptions basically follow Refs. [59] and [52]. We conservatively use a positional uncertainty of $\sigma_\theta = 0.01''$. Combining data points from several filters could be combined to give a time delay uncertainty $\sigma_{\Delta t}$ of 0.05 days for the SNAP mission. However, this number may be degraded if the lightcurve is modified by microlensing. In the following we set $\sigma_{\Delta t} = 0.15$ days. For the flux ratios, we assume the error σ_r to be dominated by microlensing [62, 63] and lensing by CDM substructure [64–66]. An error estimate of $\sigma_r/r = 0.5$ is employed. Ideally, one would like to use the proper probability distribution functions for the microlensing magnification probability as a function of, e.g. position in lens galaxy. In the following however, we assume a simple gaussian distribution and assume that extreme events with very large microlensing magnification factors can be identified from, e.g. peculiarities of the lightcurves and be removed from the sample. This will however only be true if the microlensing timescale is smaller than the timescale of the intrinsic source variations. Redshifts error are negligible; we adopt $\sigma_{z_l} = 0.001$ from photometric redshift measurements based on SNAP multi-band photometry.

Even though we can derive lensing statistics using simple spherical galaxy profiles, it is important to include lens ellipticities and galaxy environments in the analysis [67]. Motivated by models of known gravitational lens systems, we assume an uncertainty in the alignment between the mass distribution and the optical light distribution of $\langle \Delta\phi^2 \rangle^{1/2} < 10$ degrees [68]. From N-body simulations and semianalytic models of galaxy formation, we can estimate the levels of external shear due to structure near the lens in gravitational lens systems to be $\gamma_{\text{ext}} = 0.058$, with an rms dispersion of 0.071 [69]. We modify our simple simulated lensing systems to include this effect. We also add an uncertainty due to scatter in the slope of individual halos of $\Delta\eta = 0.2$.

The addition of a constant surface density κ_c to a lens, changes the time delay by a factor $1 - \kappa_c$ but leaves the image positions and flux ratios unchanged. In the following we have assumed the effects from external convergence to be comparable to or smaller than the effects from external shear and a scatter in η . However, it should be noted that the effect potentially can be very important [70, 71]. The error in the derived value of h will be directly proportional to the systematic error in the assumed value of the external shear.

When constraining h , we use a prior on the matter density of $\Omega_m = 0.30 \pm 0.04$

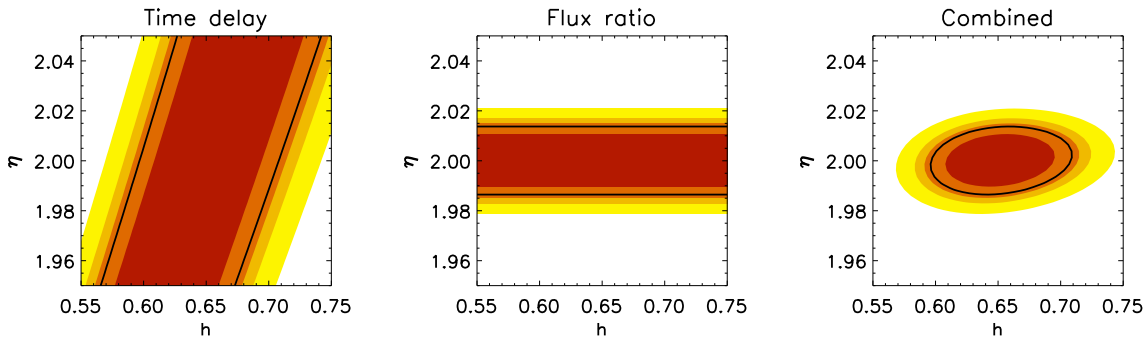


Figure 1. Constraints in the $[\eta, h]$ -plane using ~ 400 multiply imaged SNe (corresponding to a quality factor $f = 0.5$). In the left panel, constraints from the time delays are shown, in the middle panel constraints from the flux ratios. Combined constraints are shown in the right panel. Contours correspond to 68.3%, 90%, 95% and 99% confidence levels for two parameters. The black line indicates the 95% confidence level (2σ) for one parameter.

[11]. Results are very insensitive to the exact value and size of the error on this prior.

3.2. The Hubble parameter

For constraints in the $[\eta, h]$ -plane, we follow the same recipe as Ref. [52] and obtain very similar results, see Fig. 1. Small differences are due to the random fluctuations in the simulation of lens systems as well as the fact that we only include the scatter in the slope η in the uncertainty – not as a modification of the simulated sample as was the case in Ref. [52]. This is to ensure that our confidence contours are centred at the correct value to facilitate estimates of the contour sizes. Constraints from the time delays are shown in the left panel and constraints from the flux ratios in the middle panel. In deriving these constraints, we have used Eqns. (16) and (19) generalized to include the effects from galaxy ellipticities and external shear, see Appendix A. Contours correspond to 68.3%, 90%, 95% and 99% confidence levels for both parameters to have values within their borders. The black line indicates the 95% confidence level for one of the parameters to lie within the contour (i.e. 2σ). Because of the strong degeneracy in the time delay between h and η , flux ratio measurements are needed to constrain the Hubble parameter. Combining the results from the time delay and flux ratio measurements, we are able to make a determination of h within 10% and – perhaps more interestingly – to determine η at the per cent level at 95% confidence (right panel). Even for an extremely conservative value of $f = 0.05$, we can determine η within 2% and h within 25%. It should be noted however that these numbers may be severely degraded in the presence of systems with very large microlens magnifications.

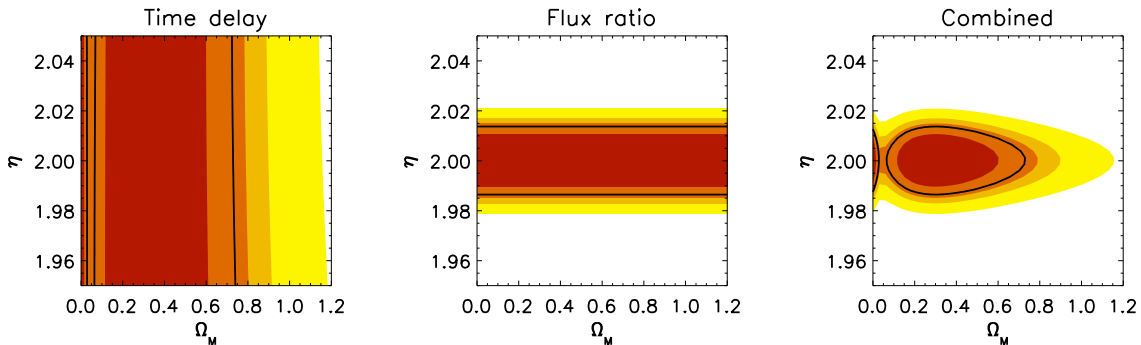


Figure 2. Constraints in the $[\eta, \Omega_M]$ -plane using ~ 400 multiply imaged SNe (corresponding to a quality factor $f = 0.5$). In the left panel, constraints from the time delay ratios are shown, in the middle panel constraints from the flux ratios. Combined constraints are shown in the right panel.

3.3. The matter density

Since the time delay is proportional to h through the distances, we can study the ratio of time delays in order to factor out the Hubble constant and constrain Ω_M (assuming a flat universe). In doing this, we wish to study ratios of lens systems with large differences in redshift in order to maximize the sensitivity of the ratio to the value of the matter density. Denoting $k_l = \Delta t_m / \Delta t_n$, where m and n numbers the lens systems in the total sample, we want to combine the time delays (i.e. choose m and n) in order to maximize $(dk/d\Omega_M)/\sigma_k \equiv k'/\sigma_k$ (i.e. maximizing the sensitivity to Ω_M). This is equivalent to maximizing the quantity

$$\frac{\Delta t'_m / \Delta t_m - \Delta t'_n / \Delta t_n}{\sqrt{\Delta t_m^{-2} + \Delta t_n^{-2}}}. \quad (20)$$

From a sample of N lens systems, we are thus able to obtain $N - 1$ time delay ratios with maximum sensitivity to Ω_M . Note the similarity of the method to the use of cross-correlation tomography in weak lensing [72]. The time delay is thus used to constrain ratios of the distance combination $(D_l D_s) / D_{ls}$, see Eq. (16). The flux ratio data is used to constrain η as described in Sec. 3.2. In Fig. 2, results from the time delays (left panel), flux ratios (middle panel) and the combined results (right panel) are shown. Note that the time delay ratios basically constrain Ω_M independent of the value of η which allows us to constrain the matter density independently of the flux ratio measurements that may be plagued by large uncertainties. The “false” minima at very low Ω_M is due to the fact that the ratio of distances often is degenerate in Ω_M . The same effect can be seen in Fig. 3 that basically probes the distance combination D_{ls} / D_s , see Eqns. (12) and (13). Though not comparable in precision to other probes of the matter density such as the LSS of galaxies, strong lensing should be able to rule out an Einstein-de Sitter universe with $\Omega_M = 1$ at very high confidence level and provide an independent sanity check of the matter density. Setting $f = 0.05$ leaves Ω_M more or less unconstrained.

4. Multiple source systems

We next compare our results obtained with single source systems with the possibility to constrain the matter density in the universe and the matter distribution in lenses using systems with multiple sources being lensed by the same lens. The cross-section for multiple imaging is larger for cluster mass lenses than for galaxy size halos. However, the time delays for cluster lenses are generally very large. Also, if the sources are galaxies, we are not able to measure the time delays. Examples of such systems are Abell 2218 [74] and Abell 1689 where 30 background galaxies are being lensed by the cluster lens and displays more than 100 images [36].

The cross-section for multiple imaging by a SIS halo is given by

$$\hat{\sigma}_{mi} = 16\pi^3 \left(\frac{v}{c}\right)^4 D_{ls}^2, \quad (21)$$

and the time delay for the two images is

$$c\Delta t = 32\pi^2 \left(\frac{v}{c}\right)^4 \frac{D_d D_{ls}}{D_s} (1 + z_l) \frac{r - 1}{r + 1} \quad (22)$$

where r is the flux ratio. For a lens redshift of $z_l = 0.5$ and a source redshift $z_s = 1.5$, we get

$$\Delta t \sim 2 \left(\frac{v}{200 \text{ km/s}}\right)^4 \frac{r - 1}{r + 1} \text{ months.} \quad (23)$$

4.1. No time delay measurements

Since the cross-section for multiple imaging is proportional to v^4 , the probability for multiple sources to be strongly lensed by a galaxy size halo is small. However, in sufficiently deep exposures of any given massive clusters, we expect to find a number of sources being lensed into multiple images. The vast majority of these sources will be galaxies in which case we will not be able to measure the time delays between images. Also, for massive cluster size lenses, time delays are generally too long to be practically observable even for variable sources. [The cross-section for two images with brightness ratio less than r is $\propto \left(\frac{r-1}{r+1}\right)^2$. Thus, we expect to observe relatively few systems with $r \sim 1$ and small time delays Δt , see Eq. (23).]

The Einstein radius is a function of both the halo slope and cosmological distances, see Eqns. (12) and (13) and in cases where we have multiple images of sources at different redshifts, we can use the observed image positions to constrain η and Ω_M . A sample of 28 multiply lensed galaxies with redshift measurements or reliable photometric redshifts behind Abell 1689 gives a constraint $\Omega_M + \Omega_\Lambda < 1.2$, i.e. the data is in accordance with an Einstein-de Sitter universe with $\Omega_M = 1$. The constraining power of the sample is limited by the low redshift ($z \sim 0.18$) of the cluster [73]. However, an analysis of four multiple image systems in Abell 2218 (also at $z \sim 0.18$) gives $0 < \Omega_M < 0.3$ assuming a flat universe, ruling out an Einstein-de Sitter universe at 5σ [74]. The difference in the claimed accuracy of the results warrants further analysis of the sensitivity of the method

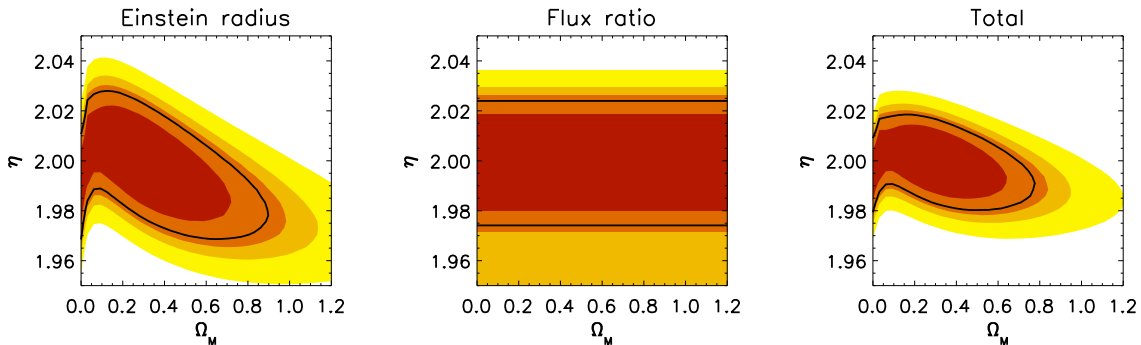


Figure 3. Results from fitting the image positions for 16 sources at regular intervals between $z = 1$ and $z = 4.75$ behind a SIS cluster at $z = 0.5$ with $v = 1000$ km/s. The uncertainty in the observed image positions is $\sigma_\theta \sim 0.2''$.

on the model assumptions and uncertainties. This question has been investigated in great detail in, e.g. Ref. [75]. Here, we investigate the sensitivity of the bound on Ω_M on the slope of the dark matter halo and the size of the observational uncertainties. We simulate a gravitational lens system consisting of a massive SIS cluster at $z = 0.5$ with $v = 1000$ km/s. We then distribute 16 sources at regular intervals between $z = 1$ and $z = 4.75$ with random source positions (inside the cross-section for multiple imaging). Note that this analysis is very primitive in the sense that we have not included any of the complexities of real cluster lenses such as substructure and departures from spherical symmetry. However, this simplicity allows us to compare the efficiency of the method compared to the ones described in Sec. 3. The accuracy of our results is completely determined by the observational error in image position. In Fig. 3, results for $\sigma_\theta = 0.2''$ is shown, yielding error contours comparable to the ones in Ref. [74] for Ω_M . Setting $\sigma_\theta = 0.5''$ basically leaves Ω_M unconstrained while $\sigma_\theta = 0.02''$ yields $\Omega_M = 0.3 \pm 0.04$ and constrains η at the per mille level*. Results for η are very sensitive to the exact source positions since large values of r dramatically improve the limits on η , see Sec. 5.

Our analysis shows that for a massive cluster with of the order 20 multiply imaged background sources at a large redshift range, we need the image positions determined to an accuracy of better than $\sigma_\theta \sim 0.2''$ to give useful bounds on Ω_M . This number can be relaxed if the number of sources is larger. The result is insensitive to any prior information on η and thus on the error in the observed flux ratios (assumed here to be $\sigma_r/r = 0.5$).

4.2. Time delay measurements

As explained in Sec. 4.1, we expect to observe very few lens systems with multiple images of several variable or transient sources with time delays short enough to be practically measurable. Nevertheless, we here explore possible constraints from such systems. In

* Of course, at this level of precision, the lens model is too crude.

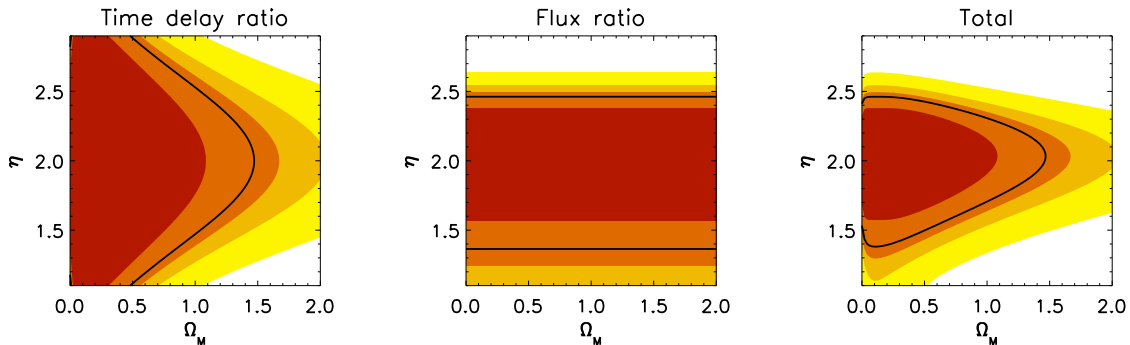


Figure 4. Results from the time delay ratio (left panel), flux ratios (middle panel) and the combined results (right panel) for a SIS lens at $z_l = 0.5$ with a velocity dispersion of $v = 300$ km/s and two multiple imaged quasars at $z_{s,a} = 1$ and $z_{s,b} = 3$ at angular source positions $\beta_a = 0.5''$ and $\beta_b = 1.0''$.

order to have a non-negligible cross-section for multiple imaging but reasonable time delays, we imagine lensing from a very heavy galaxy or a small group of galaxies. Our default system is a SIS lensing halo at $z_l = 0.5$ with a velocity dispersion of $v = 300$ km/s. We imagine two multiply imaged quasars at $z_{s,a} = 1$ and $z_{s,b} = 3$ at angular source positions $\beta_a = 0.5''$ and $\beta_b = 1.0''$. The assumed errors are the same as in Sec. 3.1 except that we set the error in the time delays to $\sigma_{\Delta t} = 2.0$ days, corresponding to typical errors for time delays between quasar images [40]. For such a configuration, we have a time delay for the images of source “a” of $\Delta t_a = 148$ days and a flux ratio of $r_a = 2.6$. The corresponding numbers for source “b” is $\Delta t_b = 296$ days and $r_b = 3.4$. We derive constraints on η and Ω_M from the observed flux ratios and the time delay ratio (c.f. Sec. 3.3), see Fig. 4. The error budget is equally shared between the error in the time delay measurements and the observational error in the image positions of $\sigma_\theta = 0.01''$. Therefore does our results not improve significantly for transient sources like SNe or gamma ray bursts where more accurate time delay measurements are possible, unless σ_θ can be significantly reduced. Note that the shape and size of the contours in the $[\eta, \Omega_M]$ -plane is very dependent on the exact configuration of the lens system. In general, results benefit from a large redshift separation for the sources since the time delay ratio is proportional to $(D_{ls}/D_s)_a/(D_{ls}/D_s)_b$. However, even in the lucky case of finding a lensing system with two well-observed multiply imaged sources with time delays determined to good accuracy, we can only hope for very rough constraints on η and Ω_M .

5. Summary and discussion

We have analyzed and compared how measurements of the image positions, flux ratios and time delays in different types of strong lensing systems will allow for the determination of the matter distribution in galaxies, as well as global cosmological parameters such as the Hubble constant h and the matter density Ω_M . While CMB

and LSS data probe properties of dark matter on large scales, measurements of galactic halos can probe the small scale properties of dark matter. Furthermore, gravitational lensing mainly probes halos at relatively high redshift where few methods for measuring galaxy density profiles are available.

First, we investigated different uses of a data set consisting of a large number of lens systems, each with a multiply imaged source with the time delay measured to high precision. Such a data set can constrain the slope of dark matter halos η at the per cent level and provides an independent test of the values of h and Ω_M . Combining the results from the time delay and flux ratio measurements, we are able to make a determination of h within 10% and η within 1% (2σ).

Factoring out the Hubble constant by studying time delay ratios, we are able to rule out $\Omega_M = 1$ at high confidence (assuming a flat universe). This bound is independent of the slope of the halos and the flux ratio measurements.

Second, we compared the results obtained for multiple systems with single sources with the use of lens systems with several multiply lensed sources in a single lens. For massive cluster size lenses, we expect to find several multiply imaged galaxy sources. The position of these images can provide a sanity check on Ω_M . The error budget is dominated by the observational error in image position that need to be of the order or less than $\sigma_\theta \sim 0.2''$ to be able to rule out an Einstein-de Sitter universe. Systems with multiply imaged sources with measurable time delays will be rare and not very useful for the purposes discussed in this paper.

In the case of a large sample of individual multiple image systems, the error budget in the time delay analysis is dominated by the observational time delay error. The flux ratio constraints are quite robust to an increase in the (gaussian) error size. Increasing the errors by a factor of 3 (to 150%), we are still able to obtain $\eta = 2 \pm 0.05$ (2σ). From Eq. (19), it is evident that systems with large flux ratios (i.e. high q) are very important when constraining galaxy density profiles since the flux ratio in these systems are more sensitive to changes in η . If such systems are absent from the sample, the error on η will increase significantly. Also, increasing the size of the external shear by a factor of ten causes a systematic bias in the determination of η of $\eta = 2 \rightarrow 1.65$. It should be noted that the use of flux ratio measurements is potentially very problematic because of large uncertainties in the microlensing magnification of individual images. Since the errors are probably not gaussian, additional information on the probability distribution of the microlensing magnifications is most likely needed in order to be able to use the flux ratio information in an unbiased way. On the other hand, observations of the microlens magnification distribution is potentially a powerful probe of the small scale structure in galaxy halos.

A possible complication is that our results for individual multiple image systems are based on the assumption that we can define average properties of lensing halos, i.e. the value of η , while N-body simulations indicate large dispersions in the individual halo properties [24–28]. Another caveat is that real lensing systems are too complicated to allow for an analysis as simplistic as in this paper. However, we are able to constrain

η and h even with a quality factor f as low as 0.05 ‡. If it is possible to retain a large number of lens systems, properties like redshift evolution of density profiles, variations in density profiles with galaxy luminosity, colour and many other important parameters can be measured by dividing the lens systems into different categories (in which also the scatter in individual halo properties may be smaller).

Undoubtedly, modelling of real future lens systems will use more complicated lens models and observational information than the one used in this paper. Nevertheless, we believe that our simple model is able to show the general parameter dependencies and approximate confidence contours that can be obtained with future strong lensing data. Since our results are fairly robust to changes in the quantity and quality of the observational data, we conclude that strong lensing should be able to give useful constraints on the matter distribution in galaxies and galaxy clusters as well as complement other cosmological probes of the Hubble parameter and the matter density.

Acknowledgments

The authors acknowledge helpful comments from an anonymous referee. EM would also like to thank the Royal Swedish Academy of Sciences for financial support.

References

- [1] Riess, A. G., et al. 1998 *Astronomical Journal* **116** 1009
- [2] Perlmutter, S., et al. 1999 *Astrophysical Journal* **517** 565
- [3] Knop, R. A., et al. 2003 *Astrophysical Journal* **598** 102
- [4] Riess, A. G., et al. 2004 *Astrophysical Journal* **607** 665
- [5] Spergel, D. N., et al. 2003 *Astrophysical Journal Supplement Series* **148** 175
- [6] Hanany, S., et al. 2000 *Astrophysical Journal* **545** L5
- [7] Netterfield, C. B., et al. 2002 *Astrophysical Journal* **571** 604
- [8] Sievers, J. L., et al. 2003 *Astrophysical Journal* **591** 599
- [9] Kovac, J. M., et al. 2002 *Nature* **420** 772
- [10] Kuo, C. L., et al. 2004 *Astrophysical Journal* **600** 32
- [11] Tegmark, M., et al. 2004 *Astrophysical Journal* **606** 702
- [12] Cole, S., et al. 2005 *Monthly Notices of the Royal Astronomical Society* **362** 505
- [13] Hannestad, S [astro-ph/0509320]
- [14] Freedman, W. L., et al. 2001 *Astrophysical Journal* **553** 47
- [15] Ratra, B., & Peebles, P. J. E. 1988 *Physical Review D* **37** 3406
- [16] Wetterich, C. 1988 *Nuclear Physics B* **302** 668
- [17] Peebles, P. J. E., & Ratra, B. 1988 *Astrophysical Journal* **325** L17
- [18] Chiba, T., Okabe, T., & Yamaguchi, M. 2000 *Physical Review D* **62** 023511
- [19] Armendáriz-Picón, C., Damour, T., & Mukhanov, V. 1999 *Physics Letters B* **458** 209
- [20] Caldwell, R. R. 2002 *Physics Letters B* **545** 23
- [21] Carroll, S. M., Hoffman, M., & Trodden, M. 2003 *Physical Review D* **68** 023509
- [22] Hannestad, S., Mörtzell, E. 2002 *Physical Review D* **66** 063508
- [23] Hannestad, S., Mörtzell, E. 2004 *Journal of Cosmology and Astro-Particle Physics* **9** 1
- [24] Navarro, J. F., Frenk, C. S., & White, S. D. M. 1997 *Astrophysical Journal* **490** 493

‡ Note however that Ω_M is left more or less unconstrained for such low values of f .

- [25] Ghigna, S., et al. 2000 *Astrophysical Journal* **544** 616
- [26] Navarro, J. F., et al. 2004 *Monthly Notices of the Royal Astronomical Society* **349** 1039
- [27] Fukushige, T., Kawai, A., & Makino, J. 2004 *Astrophysical Journal* **606** 625
- [28] Graham, A. W. et al. 2005 *Submitted to Astronomical Journal* [astro-ph/0509417]
- [29] van den Bosch, F. C., & Swaters, R. A. 2001 *Monthly Notices of the Royal Astronomical Society* **325** 1017
- [30] de Blok, W. J. G., et al. 2001 *Astrophysical Journal* **552** L23
- [31] Simon, J. D., et al. 2005 *Astrophysical Journal* **621** 757
- [32] Davis, A. N., Huterer, D., & Krauss, L. M. 2003 *Monthly Notices of the Royal Astronomical Society* **344** 1029
- [33] Cohn, J. D., et al. 2001 *Astrophysical Journal* **554** 1216
- [34] Brainerd, T. G., & Specian, M. A. 2003 *Astrophysical Journal* **593** L7
- [35] Gavazzi, R., et al. 2003 *Astronomy and Astrophysics* **403** 11
- [36] Broadhurst, T., et al. 2005 *Astrophysical Journal* **619** L143
- [37] Natarajan, P., et al. 2002 *Astrophysical Journal* **580** L17
- [38] Dahle, H., Hannestad, S., & Sommer-Larsen, J. 2003 *Astrophysical Journal* **588** L73
- [39] Refsdal, S. 1964 *Monthly Notices of the Royal Astronomical Society* **128** 307
- [40] Kochanek, C. S., & Schechter, P. L. 2004 [astro-ph/0406343]
- [41] York, T., et al. 2005 *Monthly Notices of the Royal Astronomical Society* **357** 124
- [42] Kochanek, C. S. 2002 *Astrophysical Journal* **578** 25
- [43] Kochanek, C. S. 2003 *Astrophysical Journal* **583** 49
- [44] Refregier, A. 2003 *Annual Review of Astronomy and Astrophysics* **41** 645
- [45] Hoekstra, H., Yee, H. K. C., & Gladders, M. D. 2002 *New Astronomy Review* **46** 767
- [46] Mellier, Y., et al. 2002 *SPIE* **4847** 112
- [47] Kochanek, C. S. 1996 *Astrophysical Journal* **466** 638
- [48] Falco, E. E., Kochanek, C. S., & Munoz, J. A. 1998 *Astrophysical Journal* **494** 47
- [49] Chiba, M., & Yoshii, Y. 1999 *Astrophysical Journal* **510** 42
- [50] Keeton, C. R. 2002 *Astrophysical Journal* **575** L1
- [51] Goobar, A., et al. 2002 *Astronomy and Astrophysics* **393** 25
- [52] Mörtzell, E., Dahle, H., & Hannestad, S. 2005 *Astrophysical Journal* **619** 733
- [53] Holz, D. E. 2001 *Astrophysical Journal* **556** L71
- [54] Oguri, M., & Kawano, Y. 2003 *Monthly Notices of the Royal Astronomical Society* **338** L25
- [55] Oguri, M., Suto, Y., & Turner, E. L. 2003 *Astrophysical Journal* **583** 584
- [56] Bolton, A. S., & Burles, S. 2003 *Astrophysical Journal* **592** 17
- [57] Schneider, P., Ehlers, J., & Falco, E. E. 1992 *Gravitational Lenses*, Springer-Verlag Berlin
- [58] Chang, K., & Refsdal, S. 1977 *The Evolution of the Galaxies and its Cosmological Implications* **369**
- [59] Goobar, A., et al. 2002 *Astronomy and Astrophysics* **393** 25
- [60] Goobar, A., et al. 2002 *Astronomy and Astrophysics* **392** 757
- [61] Dahlén, T., & Fransson, C. 1999 *Astronomy and Astrophysics* **350** 349
- [62] Schneider, P., & Wagoner, R. V. 1987 *Astrophysical Journal* **314** 154
- [63] Woźniak, P. R., et al. 2000 *Astrophysical Journal* **540** L65
- [64] Dalal, N., & Kochanek, C. S. 2002 *Astrophysical Journal* **572** 25
- [65] Keeton, C. R. 2003 *Astrophysical Journal* **584** 664
- [66] Mao, S., et al. 2004 *Astrophysical Journal* **604** L5
- [67] Keeton, C. R., & Zabludoff, A. I. 2004 *Astrophysical Journal* **612** 660
- [68] Kochanek, C. S. 2002 [astro-ph/0204043]
- [69] Holder, G. P., & Schechter, P. L. 2003 *Astrophysical Journal* **589** 688
- [70] Bar-Kana, R. 1996 *Astrophysical Journal* **468** 17
- [71] Oguri, M., Keeton, C. R., & Dalal, N. 2005 *Monthly Notices of the Royal Astronomical Society* **364** 1451

- [72] Jain, B., & Taylor, A. 2003 *Physical Review Letters* **91** 141302
 [73] Broadhurst, T., et al. 2005 *Astrophysical Journal* **621** 53
 [74] Soucail, G., Kneib, J.-P., & Golse, G. 2004 *Astronomy and Astrophysics* **417** L33
 [75] Dalal, N., Hennawi, J. F., & Bode, P. 2005 *Astrophysical Journal* **622** 99

Appendix A. Ellipticity and external shear

We modify our simple simulated lensing systems by adding the effects of ellipticities and shear. In order to treat possible non-sphericity of the lens systems we add a quadrupole term to the projected potential, Ψ ,

$$\Psi = \Psi_0 (1 + a \cos 2\phi), \quad (\text{A.1})$$

where Ψ_0 is the spherical potential given in Eq. (7) and ϕ is the angle of the image relative to the quadrupole axis. If the system is assumed to have relatively small ellipticity, the angle of the second image can be written as a function of the first

$$\phi_2 = \phi_1 + \pi - \delta, \quad (\text{A.2})$$

where δ is a small parameter (and explicitly zero for spherical systems).

Most lens systems are embedded within an external potential which gives rise to an additional shear contribution. We write the combined potential as

$$\Psi = \Psi_0 (1 + a \cos 2\phi) + \gamma_{\text{ext}} r^2 \cos[2(\phi - \phi_0)], \quad (\text{A.3})$$

where $\phi - \phi_0$ is the angle between the image position and the quadrupole axis of the external potential. Since γ should be small in order to justify treating the external potential as a quadrupole, we derive expressions for Δt and r which are valid to second order in q , δ and γ for arbitrary values of ϕ_0 . The expressions are given in Ref. [52]. The second order Taylor expanded expressions are excellent approximations for small q and/or $\eta \sim 2$. In practice however, we have used the full expressions for the time delays and the flux ratios. Since $\eta \sim 2$ in our simulations, the use of Taylor expansions gives close to identical results.